Supplementary Information

Hierarchical chemical bonding and multi-valley band edge induce high performance in layered $Bi_6Ag_2O_6Se_4$: A theoretical study

Ying Wang, Dongyang Wang*, Ziyu Wang*

School of Physics and Laboratory of Zhongyuan Light, Zhengzhou University, Zhengzhou 450001, China.

** Corresponding author.*

E-mail addresses:

wangdongyang@zzu.edu.cn;

wangziyu@zzu.edu.cn

Computational details

The entire calculation process, all first-principles calculations were carried out within the framework of Density Functional Theory (DFT) using the Vienna Ab initio Simulation Package (VASP)[1], with the Generalized Gradient Approximation (GGA) and the Projector Augmented Wave (PAW) method[2, 3]. The Perdew-Burke-Ernzerhof revised for solids (PBEsol)[4] functional was adopted to handle the exchange-correlation interactions. The cut-off energy for PAW was set to 450 eV, and the Brillouin zone was sampled using a 13 × 13 × 2 grid centered at the Γ point. Both the lattice parameters and atomic coordinates were fully relaxed, with the convergence thresholds for the total energy and Hellmann-Feynman atomic forces set to 10^{-8} eV and 10^{-4} eVÅ^{-1}, respectively.

The electronic band structure was calculated using the modified Beck-Johnson (mBJ)[5] potential, which can achieve accurate band gaps comparable to expensive hybrid function[6]. Since the PBEsol (~0.30 eV) functional underestimates the bandgap, the mBJ (~1.19 eV) functional can describe the bandgap more accurately. Therefore, the mBJ functional was adopted to calculate the carrier transport properties.

To explore the bonding strength of $Bi_6Ag_2O_6Se_4$, the Crystal Orbital Hamilton Population (COHP)[7] analysis was conducted *via* the LOBSTER code, with the employment of Bunge basis sets.

The ab initio molecular dynamics (AIMD)[8] simulations based on the canonical ensemble (NVT) were performed at temperatures of 50 K, 300 K, 400 K, 500 K, 600 K, 700 K, and 800 K, with the time step 2 fs and total simulation time 8 ps, respectively.

To accurately calculate the interatomic interaction forces for phonon transport in $Bi_6Ag_2O_6Se_4$, the Moment Tensor Potential (MTP)[9, 10] method is adopted, as implemented in the Machine Learning Interatomic Potentials (MLIP) package[10]. Energies, forces, and stresses were extracted from the AIMD simulations to train the MTP by solving the minimization problem implemented in the MLIP software. The weights of energy, force, and stress were set to 1.0, 0.1, and 0.001, respectively. On this basis, a 5 × 5 × 1 supercell was constructed to extract the second- and third-order

interatomic force constants (IFCs). The third-order force constants were extracted with the cutoff radius up to 10 nearest-neighbor atoms. After obtaining the IFCs, the phonon dispersion and density of states can be obtained using the Phonopy package[11].

The atomic displacement parameters (ADP) were calculated based on the formula:

$$\langle |u(jl,t)|^2 \rangle = \frac{\hbar}{2Nm_j} \sum_{q,\upsilon} \omega_\upsilon(q)^{-1}(1 + 2n_\upsilon(q))|\hat{n}\cdot e_\upsilon(j,q)|^2$$

Where $\hat{n}$ is an arbitrary unit direction, *j* and *l* are the labels for the *j*-th atomic position in the *l*-th unit cell, *t* is the time, m_j is the atomic mass, *N* is the number of the unit cells, **q** is the wave vector, υ is the index of phonon mode. $\omega_\upsilon(\mathbf{q})$ is the phonon frequency, $n_\upsilon(\mathbf{q})$ is the phonon population and $e_\upsilon(j,\mathbf{q})$ is the polarization vector of the atom *jl* and the band υ at **q**.

The ShengBTE software[12] was used to calculate the lattice thermal conductivity through iteratively solve the phonon Boltzmann transport equation. The introduction of four phonon scattering usually reduces the lattice thermal conductivity, but the degree of influence on the thermal conductivity varies[13]. For instance, it can be reduced by 36% in BAs[14], but in some systems, the impact is negligible in diamond[14, 15]. Thus, considering the giant demand of computational resources[14, 16] for a larger system of $Bi_6Ag_2O_6Se_4$, only the three-phonon scattering process was included. We carefully examined the convergence of lattice thermal conductivity with respect to the *q*-grid. The *q*-grid was tested and found the convergence, as shown in **Fig. S4**. And the transport properties were calculated based on a 13 × 13 × 4 *q*-grid.

To accurately evaluate the carrier relaxation time and transport properties, the AMSET software package[17] was adopted in this work. The AMSET software package considers three key scattering mechanisms: elastic ionized impurity (IMP) scattering, elastic acoustic deformation potential (ADP) scattering, and inelastic polar optical phonon (POP) scattering, yielding reasonable carrier relaxation times. This software is widely applied to two-dimensional structural and layered structural thermoelectric materials[18, 19].

Tables and Figures

Table S1. The effective mass (m_e) and band degeneracy for VBM and CBM.

	m^* (m_e)	N_v
VBM	0.766	4
CBM	0.417	1

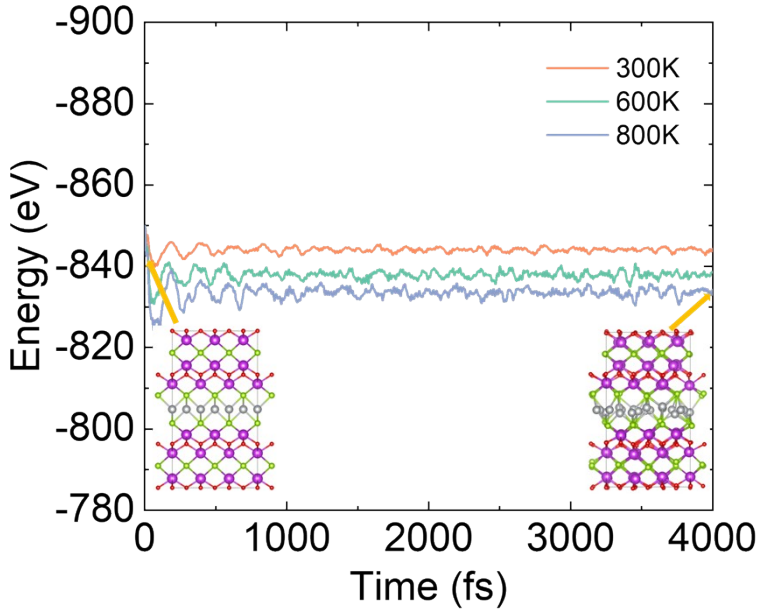

Fig. S1 AIMD simulations of $Bi_6Ag_2O_6Se_4$ at 300 K, 600 K, and 800 K as a function of timestep. The inserts represent the initial and the final structures $Bi_6Ag_2O_6Se_4$ at 800 K. There is no obvious bond reconstruction, suggesting the thermodynamic stability of $Bi_6Ag_2O_6Se_4$ until the 800 K.

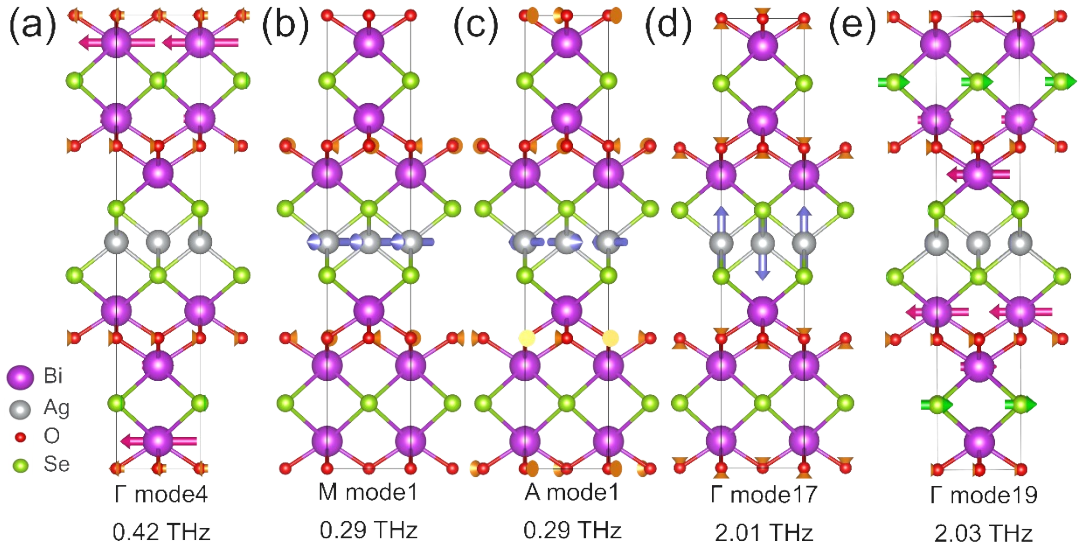

Fig. S2 Visualized phonon eigenvectors of the lowest phonon mode at (a) Γ point, (b) M point, (c) A point. (d) and (e) are the phonon mode corresponding to the peaks for the PDOS of Ag and Bi atoms. The arrow length refers to the vibration amplitude.

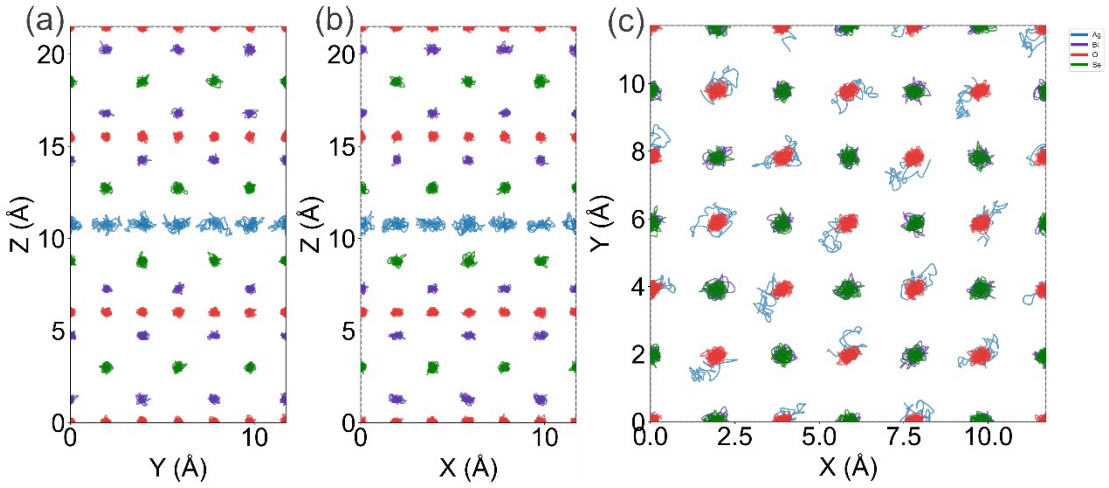

Fig. S3 The atomic trajectory of $Bi_6Ag_2O_6Se_4$ at 600 K along (a) *x* axis, (b) *y* axis, and (c) *z* axis.

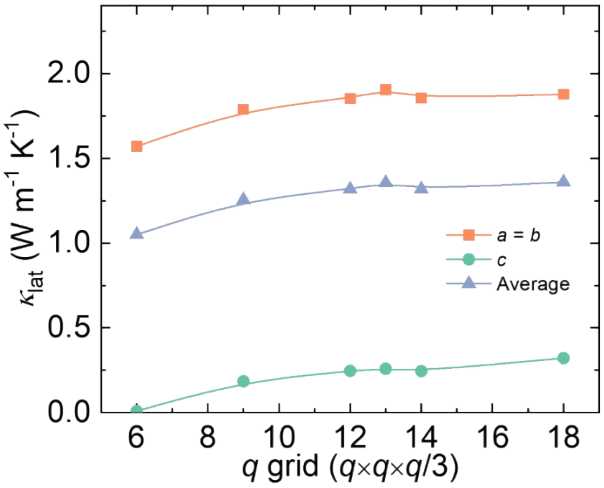

Fig. S4 Convergence test of lattice thermal conductivity with different *q*-grid of $Bi_6Ag_2O_6Se_4$. The 13 × 13 × 4 *q*-point mesh used in our calculations show the relative error smaller than 2.8 %.

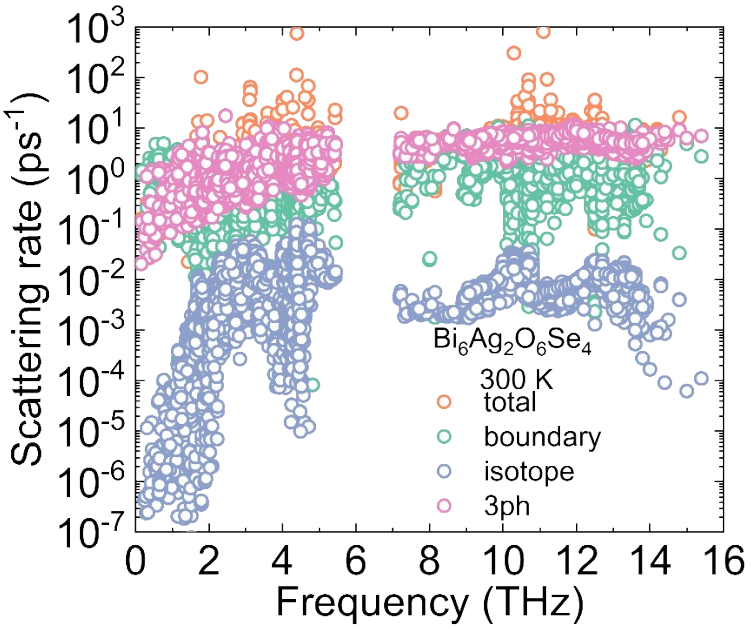

Fig. S5 Calculated the total scattering rate of $Bi_6Ag_2O_6Se_4$, and the contribution from boundary, isotopic, and three-phonon (3ph) scattering mechanisms.

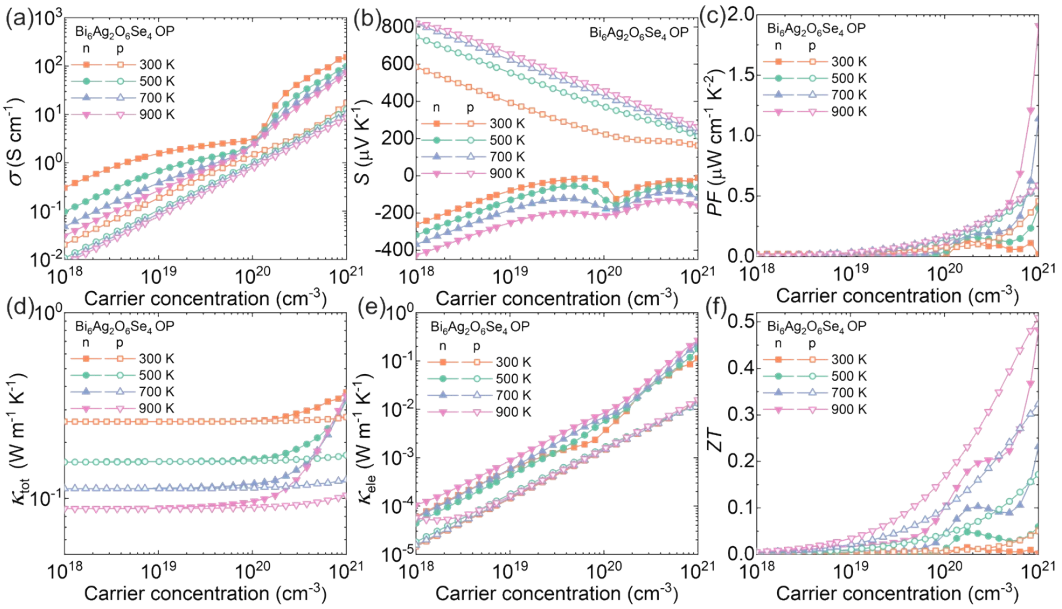

Fig. S6 Evaluated thermoelectric properties of *n*-type (solid symbols) and *p*-type (hollow symbols) doped $Bi_6Ag_2O_6Se_4$ along the out-of-plane (OP) directions at 300 K, 500 K, 700K, and 900 K. (a) Electrical conductivity (σ), (b) Seebeck coefficient (S), (c) power factor (PF), (d) total thermal conductivity (κ_{tot}), (e) electronic thermal conductivity (κ_{ele}), and (f) figure of merit (ZT).

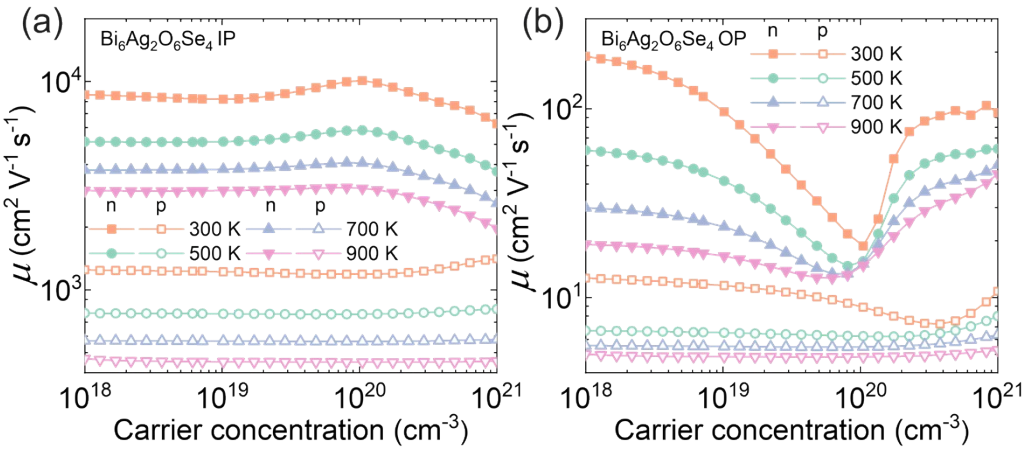

Fig. S7 Predicted the carrier mobility of *n*-type (solid symbols) and *p*-type (hollow symbols) doped $Bi_6Ag_2O_6Se_4$ along (a) in-plane (IP) and (b) out-of-plane (OP) directions at 300 K, 500 K, 700K, and 900 K.

References

1. J. Hafner, *J. Comput. Chem.*, 2008, **29**, 2044-2078.
2. J. P. Perdew, K. Burke and M. Ernzerhof, *Phys. Rev. Lett.*, 1996, **77**, 3865-3868.
3. P. E. Blöchl, *Phys. Rev. B*, 1994, **50**, 17953-17979.
4. J. P. Perdew, A. Ruzsinszky, G. I. Csonka, O. A. Vydrov, G. E. Scuseria, L. A. Constantin, X. Zhou and K. Burke, *Phys. Rev. Lett.*, 2008, **100**, 136406.
5. J. A. Camargo-Martínez and R. Baquero, *Phys. Rev. B*, 2012, **86**, 195106.
6. J. Heyd and G. E. Scuseria, *J. Chem. Phys.*, 2004, **121**, 1187-1192.
7. J. George, G. Petretto, A. Naik, M. Esters, A. J. Jackson, R. Nelson, R. Dronskowski, G.-M. Rignanese and G. Hautier, *ChemPlusChem*, 2022, **87**, e202200123.
8. M. E. Tuckerman, P. J. Ungar, T. von Rosenvinge and M. L. Klein, *J. Phys. Chem.*, 1996, **100**, 12878-12887.
9. A. V. Shapeev, *Multiscale Model. Sim.*, 2016, **14**, 1153-1173.
10. I. S. Novikov, K. Gubaev, E. V. Podryabinkin and A. V. Shapeev, *Mach. Learn.: Sci. Technol.*, 2021, **2**, 025002.
11. A. Togo and I. Tanaka, *Scripta Mater.*, 2015, **108**, 1-5.
12. W. Li, J. Carrete, N. A. Katcho and N. Mingo, *Comput. Phys. Commun.*, 2014, **185**, 1747-1758.
13. Z. Guo, Z. Han, D. Feng, G. Lin and X. Ruan, *Npj. Comput. Mater.*, 2024, **10**, 31.
14. T. Feng, L. Lindsay and X. Ruan, *Phys. Rev. B*, 2017, **96**, 161201.
15. Z. Han and X. Ruan, *Phys. Rev. B*, 2023, **108**, L121412.
16. T. Feng and X. Ruan, *Phys. Rev. B*, 2016, **93**, 045202.
17. A. M. Ganose, J. Park, A. Faghaninia, R. Woods-Robinson, K. A. Persson and A. Jain, *Nat. Commun.*, 2021, **12**, 2222.
18. T. Yue, Y. Zhao, J. Ni, S. Meng and Z. Dai, *Npj. Comput. Mater.*, 2023, **9**, 17.
19. D. Wang, K. Zhao, T. Hong, J. Zhu, H. Shi, B. Qin, Y. Qin, G. Wang, X. Gao, S. Cheng, C. Shan and L.-D. Zhao, *Mater. Today Phys.*, 2025, **51**, 101654.